1965

Experimental studies of the moment-curvature-thrust relationship, The Welding Journal, Vol. 44, Feb. 1965, Publication No. 258/65-1

M. G. Lay

N. Gimsing

LEHIGH UNIVERSITY INSTITUTE OF RESEARCH

Plastic Design in High Strength Steel

FURTHER STUDIES OF THE MOMENT-THRUST-CURVATURE RELATIONSHIP

by

Maxwell G. Lay
Neils Gimsing

Fritz Engineering Laboratory Report No. 297.4

Plastic Design in High Strength Steel

FURTHER STUDIES OF THE MOMENT-THRUST-CURVATURE RELATIONSHIP

by

M. G. Lay
N. Gimsing

This work has been carried out as part of an investigation sponsored jointly by the Welding Research Council and the Department of the Navy with funds furnished by the following:

American Institute of Steel Construction
American Iron and Steel Institute
Institute of Research, Lehigh University
Column Research Council (Advisory)
Bureau of Ships (Contract No. Nobs 90041)
Bureau of Yards and Docks (Contract No. NBy 53160)
Welding Research Council

January 1964

Fritz Engineering Laboratory
Department of Civil Engineering
Lehigh University
Bethlehem, Pennsylvania

Fritz Engineering Laboratory Report No. 297.4

SYNOPSIS

The relationship between bending moment, axial force and curvature is basic to the study of structures. The problem has been solved theoretically in a number of ways, but the experimental aspect has received less attention. This report gives some experimental confirmation of the predicted behavior.

It is found that, on an overall scale, the existing theories provide an adequate representation of the behavior, although allowance must be made for the occurrence of local buckling. On a localized scale the agreement between test and theory is not consistently reliable, and it becomes apparent that the overall theory is an average representation of the number of dissimilar conditions. However, this average representation appears adequate for most structural purposes.

TABLE OF CONTENTS

I. INTRODUCTION

The deformations which occur when a cross-section is subjected to axial force and bending moment will be planar on the elastic regime[1], and it is customary to assume that the deformations remain planar after yielding has occurred. The situation is shown in Fig. 1 where P is the axial force and M is the bending moment. The deformed plane is represented by the average or centerline axial strain ϵ_o and the curvature or gradient, ψ, of the deformed plane with respect to its original location. Thus the strain, ϵ, at any location on the cross-section distant y from the centerline is

$$\epsilon = \epsilon_o + \psi \cdot y \tag{1}$$

The problem is to determine M and P for given values of ϵ_o and ψ, or vice versa. It is solved by relating strains, ϵ, to stresses, σ, by the stress-strain law;

$$\sigma = \sigma(\epsilon) = \sigma(\epsilon_o + \psi \cdot y) \tag{2}$$

and integrating over the cross-section to obtain the internal loads P_i and M_i;

$$P_i = \int_A \sigma(\epsilon_o + \psi y)\, dA \tag{3}$$

$$M_i = \int_A y\,\sigma(\epsilon_o + \psi y)\, dA \tag{4}$$

By equilibrium $P = P_i$ and $M = M_i$.

The solution of equations (3) and (4) present no mathematical difficulty. The difficulties are of a manipulative nature and arise from the following factors:

1) Residual strains. Residual strains, ϵ_{r_0}, may exist in the cross-section and are a function of their location, that is $\epsilon_r = \epsilon_r(y,x)$. This requires that the stress-strain law be amended to

$$\sigma = \sigma(\epsilon + \epsilon_r) = \sigma(x,y) \qquad (5)$$

2) Cross-sectional shape. The application of the integrals in equations (3) and (4) to a typical wide-flange shape requires a piecewise integration process.

II. ANALYTICAL SOLUTIONS

The solution to the simplest case of a rectangular section and an elastic-plastic stress-strain law (Fig. 2), has been known for many years[2]. Algebraic relationships are established between M, P, ψ and ϵ_o for each yielding configuration and these are then solved within their particular limits.

The complexities of this approach for wide-flange sections containing residual strains led Ketter et al[3] to introduce a variation of the technique in which the moment and force are found for a certain number of well chosen strain distributions. Intermediate values of the parameters are obtained by interpolation.

The increasing availability of high speed computers has allowed the circumvention of the tedious algebraic evaluations. Fukumoto[4] has recently produced programs and solutions for the wide-flange shape ideal-

ised to three rectangles and containing the residual strains shown in Fig. 3. The value of α occurring in the tensile residual strains is chosen to achieve axial eqiulibrium under zero external load (usually $\alpha \approx 0.6$).

Computers can solve the given algebraic equations but they cannot set them up. Furthermore, the presence of a non-linear residual strain pattern and of yield stresses varying between web and flange and tension and compression, can make even the algebraic statement of the problem a considerable task. There is, therefore, considerable merit in a recent computer method developed by Birnstiel and Michalos[5] for a still more complex situation.

In this method, the section is divided into a number of sub-areas, A_s, with co-ordinates (x_s, y_s), residual strain ϵ_{rs} and yield strain σ_{ys} (Fig. 4). The integration in equations (3) and (4) is then reduced to a machine summation:

$$P_i = \sum_A \sigma(\epsilon_{rs} + \epsilon_o + \psi y_s) \tag{6}$$

$$M_i = \sum_A y_s \, \sigma(\epsilon_{rs} + \epsilon_o + \psi y_s) \tag{7}$$

The ease of solution is now almost independent of the residual strain pattern, the yield stress variation, and the cross-sectional shape. A difficulty is that the subdivision size must be sufficiently small not to obscure the significant effects which result when the neutral axis ($\epsilon = 0$) is in the flange.

III. A PARTICULAR SOLUTION

It is convenient in the analysis of later experimental results to have available a simple solution capable of accounting for variations in yield stress and of algebraic manipulation. In the zone of most interest to this study, the applied strains will be large relative to the residual strains. Hence the residual strain distribution, in Fig. 3 is approximated by assuming an average compressive residual strain of $\epsilon_{rf} = 0.5\ (1-\alpha)(0.3\epsilon_y)$. For the section dimensions shown in Fig. 5a this reduces to

$$\epsilon_{rf} = \frac{1}{2}\ (0.3\epsilon_y)\ \frac{1}{1 + \frac{bt}{w(d-2t)}} \tag{8}$$

The new residual strain pattern is also shown in Fig. 5a.

If the yield stress of the flange is σ_{yf} and of the web σ_{yw}, the effective yield stresses become

Flange in compression: $\sigma_c = \sigma_{yf} - E\epsilon_{rf}$ (9a)

Web in compression: $\sigma_w = \sigma_{yw} + E\epsilon_{rw}$ (9b)

Flange in tension: $\sigma_t = \sigma_{yf} + E\epsilon_{rf}$ (9c)

A method analogous to that of Ketter et al[3] is used. The two major yielding cases are shown in Fig. 5b and occur when the tension flange is elastic (case 1) and when it is yielded in compression (case 2). The relationship between moment and axial force is assumed linear and given by

$$M = Pe \tag{10}$$

The value of P is then

Case 1. $$\frac{P}{A} = \frac{\sigma_w - \frac{bt}{A}(\sigma_w - \sigma_c)\left(1 + \frac{1}{2}\,\frac{1 - t/d}{0.5 - \eta z/d}\right)}{1 + \frac{e/d}{1/2 - \eta z/d}} \tag{11a}$$

Case 2. $$\frac{P}{A} = \frac{\sigma_w - \frac{2bt}{A}(\sigma_w - \sigma_c)}{1 + \frac{e/d}{1/2 - \eta z/d}} \tag{11b}$$

where:

Case 1. $$\eta = 1 - \frac{2}{3}\,\frac{1 - (1 - \frac{w}{b})(1 - \frac{t}{d}(\frac{d}{z}))^3}{1 - (1 - \frac{w}{b})(1 - \frac{t}{d}(\frac{d}{z}))^2} \tag{12a}$$

Case 2. $$\eta = \frac{1}{3} \tag{12b}$$

and z/d is a parameter related to the amount of yielding (Fig. 5b). The curvatures are found from

Case 1. $$\frac{\psi}{\psi_y} = \frac{A}{bd}\cdot\left(\frac{d}{z}\right)^2 \cdot \frac{\frac{\sigma_w}{\sigma_c} + \frac{bt}{A}\cdot\frac{d}{e}\cdot\left(\frac{\sigma_w}{\sigma_c} - 1\right)\left(\frac{1}{2} - \frac{e}{d} - \frac{1}{2}\frac{t}{d}\right)}{\left(1 - (1 - \frac{w}{b})(1 - \frac{t}{d}\cdot\frac{d}{z})^2\right)\left(\frac{1}{2} + \frac{e}{d} - \eta\frac{z}{d}\right)} \tag{13a}$$

Case 2. $$\frac{\psi}{\psi_y} = \frac{A}{bd}\cdot\left(\frac{d}{z}\right)^2 \cdot \frac{\frac{\sigma_w}{\sigma_c} - \frac{2bt}{A}\left(\frac{\sigma_w}{\sigma_c} - 1\right)}{1 + \frac{\frac{1}{2} - \frac{1}{3}\frac{z}{d}}{e/d}} \tag{13b}$$

The moments are given by equation (10) and the axial strains, ϵ_o, by:

$$\epsilon_o = \epsilon_y + \frac{\psi}{\psi_y}\left(1 - 2\frac{z}{d}\right)\epsilon_c \tag{14}$$

where $\epsilon_y = \epsilon_w$ (Case 1) and $\epsilon_y = \epsilon_c$ (Case 2).

Solutions are obtained by varying z/d. For Case 1:

$$\frac{t}{d} < \frac{z}{d} < 1 - \frac{t}{d} \tag{15a}$$

and for Case 2, $$0 < \frac{z}{d} < \frac{t}{d} \tag{15b}$$

There is an insignificant case between Cases 1 and 2, and both cases become invalid if tensile yielding occurs, that is if

$$\frac{\psi}{\psi_y} \cdot \frac{z}{d} < \frac{\epsilon_y + \epsilon_T}{2\epsilon_c} \tag{16}$$

In the above equations, $\psi_y = 2\epsilon_c / d$ (17)

IV. ULTIMATE CONDITIONS

The maximum moment and axial force which a section can carry are inter-related and the condition is denoted by (M_{pc}, P_{yc}). Expressions for M_{pc} in terms of P_{yc} are available[6] for sections with a uniform yield stress. A similar expression for non-uniform yield stress will be presented here. Use will be made of equation (10) to relate M_{pc} and P_{yc}.

Analogous to Cases 1 and 2 in the preceding section, it is necessary to distinquish between the neutral axis being in the web or in the tension flange. It is in the flange if

$$\frac{P}{P_y} > \frac{1}{1 + \frac{2bt}{(d-2t)w} \cdot \frac{\sigma_c}{\sigma_w}} \tag{18}$$

This limit varies between 0.19 and 0.56 for WF sections but lies between 0.20 and 0.35 for most column sections. For example, the limit is 0.29 for the 14WF78 and 0.31 for the 8WF31. As the low axial load values are not relevant to this discussion, the following equations are restricted to the neutral-axis-in-flange case. It is useful to define the constant B where

$$B = 1 + \frac{2bt}{(d-2t)w} \cdot \frac{\sigma_c}{\sigma_w} \cdot \frac{1}{1 + \frac{\sigma_t}{\sigma_c}} \tag{19}$$

The following equations apply to the situation in which

$$1 \gg B \cdot \frac{4 \cdot \frac{t}{d} \cdot \frac{e}{d}}{\left(\frac{1}{2} + \frac{e}{d}\right)^2} \tag{20}$$

The following equations are derived in an identical manner to those in Reference 6. The distance, (a)t, of the neutral axis from the outer face of the tension flange (Fig. 6) is given by

$$(a)t = \frac{2B}{1 + \frac{1}{2} \cdot \frac{d}{e}} < t \tag{21}$$

and the axial force P_{yc} is

$$\frac{P_{yc}}{P_y} = \frac{1}{1 + 2\frac{e}{d}} \tag{22}$$

In the above equations

$$P_y = 2bt\sigma_c + (d - 2t)w\sigma_w \tag{23}$$

V. EXPERIMENTAL STUDIES

The most direct means of experimentally studying the moment-force-curvature relationship is by means of the eccentric stub-column test. Such tests have previously been reported by Driscoll and Beedle[7], and Hendry[8] has conducted similar tests. The testing arrangement used by Driscoll and Beedle is shown in Fig. 7. The end fixtures have been described elsewhere[9].

Two additional tests will be described in this report. These tests used the same testing arrangement as had been used by Driscoll and Beedle (Fig. 7). They differ from the previous tests in that the sec-

tions tested were column rather than beam sections* and in that the specimens were extensively strain gaged (Fig. 8). The strain gages allowed a close check on the strain distributions occurring during the loading sequence.

Details of the eccentric stub column tests performed by Driscoll and Beedle and by the authors are given in Table 1. The cross-sectional dimensions given are measured values. The experimental data for tests T-7 and T-8 (Ref. 7) consist of the relationships between moment and curvature and are available elsewhere[7,10]. The results agree closely with the given theoretical calculations.

VI. TEST RESULTS - HT SERIES

INTRODUCTION

This section will discuss the detailed results of the HT series tests described in Table 1. The testing arrangement used is shown in Fig. 7 and the instrumentation is shown in Fig. 8. The tests were conducted at a slow strain rate and at each reading the strain rate was stopped completely. No readings were taken until the yielding process had stopped. This usually took about five to ten minutes. The tests were conducted in a mechanical screw loading testing machine.

---

* A column section will be defined as one in which $b > 0.75d$, a beam section as one in which $b < 0.75d$.

The major numerical results of the two tests are given in Table 2. The basic moment-curvature relationships are plotted in Figs. 9a and 9b for tests HT-18 and HT-2, respectively. The curvature used in obtaining these graphs is the average overall curvature. From Fig. 8 it can be seen that this is

$$\psi_{av} = \theta/L \tag{24}$$

The theoretical predictions are obtained from Section IV.

Before severe local bukcling occurs, the agreement between test and theory is well within normal structural limits. The initial occurrence of local buckling has no observable effect on the test behavior, but after a further curvature increase of the order of 0.00035 in^{-1} unloading and severe local buckling occurred in both tests. The moment-curvature relationship can thus be considered valid up to this point of severe local buckling.

The estimate of M_{pc} will consequently be made non-conservative by the occurrence of local buckling. This also applies for beams but in that case the difference in moments is negligible as it is proportional to the web thickness, w, (the neutral axis being in the web). For columns, the neutral axis will usually be in the flange (equation 18) and therefore the difference in moments will be proportional to the breadth of the flange, b. In the cases represented by tests HT-18 and HT-2, the difference between M_{pc} and the theoretical moment at unloading is 1.5% and 3% respectively. The larger difference for HT-2 is a result of the relatively earlier occurrence of local buckling in that test. Clearly, the reduction in moment capacity is still negligible for the sections tested.

Further information can be obtained from Figs. 9. The initial parts of the curves are linear (slope = $\arctan EI$). They show a marked departure from linearity once the compression flange is fully yielded and the yielding begins to move into the web. This is to be expected as most of the resistance of the section is supplied by the flanges. General yielding of the flanges can be calculated to have occurred at flange stress levels of 48 ksi for HT-18 and 45 ksi for HT-2. The residual stress levels can be estimated by subtracting these values from the flange yield stresses (σ_{yf} in Table 1); the results are 6 ksi and 8 ksi respectively. The measured residual stresses* at the flange tips averaged 7 ksi and would seem to confirm the experimental observations.

The behavior of the member under combined axial force and moment is well illustrated by the series of photographs shown in Fig. 10 These were taken during test HT-18 and the numbers correspond to the numbers on the graph in Fig. 9a. The photographs make very clear the discontinuous nature of the yielding process and it is obvious that any theory based on a continuous behavior assumption (such as that discussed in this report) can only give approximations to the true behavior.

The yield lines are seen to congregate into large slip bands at 45° to the load axis. However, at local buckling (Fig. 10d and e) the entire region is crossed by yield lines.

LOCAL BUCKLING

The preceding discussion has made it clear that the validity of the theoretical predictions depends on the absence of severe load buckling.

---

* Tests HT-19 and HT-9, Project 297

The strains at the point of observed local buckling and at unloading (severe local buckling) are plotted in Fig. 11. The figures show the strain distribution over the compression flange in terms of bar graphs. The strain values are recorded alongside the top of the bar graphs. The solid bars represent the strains when local buckling was observed. The open bars are the strains at unloading. The gage locations correspond to the base of the bars. The strain hardening strain for this steel** is 0.019.

The accepted local buckling theory[11] predicts that, for A36 steel, local buckling of a flange will not occur until it is fully strain hardened, provided that its b/t value satisfies

$$\frac{b}{t} \leqslant 17 \tag{25}$$

As this is a buckling solution it is reasonable to modify it for other steels by the square root of the yield stresses

$$\frac{b}{t} \leqslant 17\sqrt{\frac{36}{\sigma_y}} \tag{26}$$

which becomes for A441

$$\frac{b}{t} \leqslant 14.4 \tag{27}$$

Both the sections tested have b/t values exceeding 14.4 (see Table 1) and so would be expected to buckle at strains below strain-hardening. This is confirmed by the results shown in Figs. 11 where local buckling was observed at centerline strains of 68% strain-hardening

** Tests HT-3 to 6 and HT-22 to 25, Project 297

for HT-18 (b/t = 16.6) and 40% strain-hardening for HT-2 (b/t = 19.6). However, buckling did not cause immediate unloading, and in each case there was appreciable post-buckling strength. For HT-18 this was sufficient to allow attainment of strain-hardening strains at the centerline and in HT-2 the centerline strain was 84% of strain-hardening. It would, therefore, appear that the buckling solution of equation (26) may be overly conservative in some cases.

The reason for the occasional low strains (such as the lower left gage in Fig. 11a) can be seen by observing the yield line pattern in Fig. 10. There is a possibility that the gages may be situated on elastic islands and therefore record elastic local strains although the average strain along the section would be much greater.

STRAIN DISTRIBUTIONS

Test-versus-theory curves such as those in Fig. 9 provide overall confirmation of the analytical approach. Localized verification is obtained from an examination of the recorded strain distributions. The strains to be discussed will be those recorded at midheight of test HT-18. There were three gages on the compression flange, two on the web at the centerline and two on the tension flange (Fig. 8). The strains recorded across the compression flange are shown in Fig. 12, the numbers corresponding to the load numbers in Fig. 9a.

The lack of any regularity in these strain distributions again emphasizes the approximate nature of the assumption of uniform behavior. The distribution at load #21 (Fig. 12) results from the right hand gage

being so located that no yield lines have passed through its gage length. The distribution at load #26 (Fig. 12) results from the effect of the unsymmetrical local buckle, which can be seen in Fig. 10e.

The strain distribution across the section is shown in Fig. 13. In this case the strains plotted for each location are the mean values of the gage readings at that distance from the centerline; for example, the compression flange value is the mean of the three strains plotted in Fig. 12. The numbers correspond to the load numbers in Fig. 9a.

The resultant strain distributions depart from linearity once yielding has occurred. This is due to the random nature of the yielding process, as the reading of any gage depends on its location in the yield line pattern. The tension flange gages remain elastic and will not be affected by these factors. The compression flange strain is the mean of three gages five inches apart and should be reasonably reliable. However, the web reading is the average of two gages separated only by the thickness of the web and its strains will, therefore, be extremely localized. In deriving subsequent stress blocks when web gages have yielded, the strain distribution will be taken as a straight line connecting the gage readings on both flanges. This approach assumes that, overall, plane sections do remain close to plane, even in a yielded region. There is some justification for this because as the section becomes more deformed -- and the yielding less random -- the strain distributions in Fig. 13 tend to return to a linear form.

Then, by using the values of σ_c and σ_w from Table 1 for the flange and web yield stresses, the stress distributions in Fig. 14 are obtained. This figure shows excellent agreement with the visual observations recorded on Fig. 9a and shown in the photographs in Figs. 10. The first yield (#14) occurs at a level below σ_c as σ_c was calculated (Equation 9a) on the assumption of a uniform compressive residual stress in the flange of 2 ksi whereas the stress at the flange tip was about 7 ski above this. The points at which the various stages of web yielding were observed (#16, 18 and 24) correspond closely to the predicted yield penetrations in Fig. 14.

The parameter z used in Section III, and defined in Fig. 5, can be directly read from Fig. 14. For instance, $z/d = 0.292$ for load #21. The tension flange stress corresponding to this value can then be calculated from equation 13a and checked against the experimental value. These theoretical predictions are shown by the dashed lines in Fig. 14 and correspond to curvatures which are slightly less than the experimental values.

It is not feasible to directly check moments against the stress distributions shown, as once yielding enters the web any changes in moment are very small and the solutions become ill-defined. It is of interest to note the common intersection point of the stress distributions in Fig. 14.

The location of the neutral axis can be examined. Figure 15 is a plot of the neutral axis location against the overall curvature (Eq. 24). The neutral axis is seen to lie close to the elastic predic-

tion until yielding progresses into the compression flange. As the section moment-curvature diagram passes around the knee in the curve (Fig. 9a), the neutral axis moves rapidly toward the flange of the member. During further deformation under almost constant moment the neutral axis approaches closely its predicted location at ultimate load.

Using curvature, which is a well defined quantity, it is possible to directly compare test and theory with respect to the neutral axis location. With the symbols of Section IV, the distance of the neutral axis from the centerline is given by

$$\beta = \frac{1}{2} - \frac{z}{d} + \left(\frac{\psi_y}{\psi}\right) \frac{\sigma_w}{\sigma_c + \sigma_T} \qquad (28)$$

and z/d is given as a function of ψ/ψ_y in equation (13a).

From Fig. 15 it is apparent that the test and theory curves follow a similar form but the theory predicts significantly larger values, at the same curvature, for the distance between neutral axis and centerline. When the discontinuous nature of the processes involved are considered, it is not surprising that there are some differences between test snd theory when localized behavior is investigated. For instance, a better comparison would be obtained if the neutral axis location were plotted against the local section curvature, rather than the average curvature. However, it is more realistic, structurally, to compare results with overall rather than localized deformations.

AXIAL DEFORMATION

In Section I it was pointed out that, whereas structural practice usually considers only moment-axial force-curvature, the axial deformation at the centerline, ϵ_o, is also a necessary term in

the definition of the deformed shape of the cross-section. Using the symbols of Section III, this strain, ϵ_o, is given parametrically as

$$\epsilon_o = \epsilon_w + \left(1 - 2\frac{z}{d}\right)\cdot\frac{\psi}{\psi_y}\cdot\epsilon_c \qquad (29)$$

and equation (13a) is used to eliminate parameter z/d.

The experimental relationship between ϵ_o/ϵ_w and ψ/ψ_y is given in Fig. 16. This result is typical of the previous data. The initial agreement (loads below #15) between elastic theory and experiment is excellent. In the range in which the section is partially yielded (Fig. 10) the experimental curve vacillates between the values of the elastic and inelastic theories in an apparently random manner. Once yielding becomes uniform (load #24 onwards) the test result tends to follow the predictions of the post-elastic theory.

It should be noted from Fig. 16 that the commonly neglected axial deformation is not insignificant. For the instance shown the deformation at local buckling was 4.5 times the yield deformation. Although this would only occur over the length of a plastic hinge in a real structure, its effect on the load distribution could still be appreciable.

VII. SUMMARY

The various theories used to predict the moment-axial force-curvature relationship for wide-flange sections have been described and their implications discussed. There is seen to be no difference in the

concepts involved and all assume a uniform stress-strain relationship. A method suitable for handling non-uniform problems has been proposed.

A second analytical method has been presented which is applicable in the almost horizontal portion of the load-deformation curve. This method is amenable to rapid hand calculation and also has the advantage of allowing strain and stress distributions to be readily found.

Previous experimental studies have been reviewed. These are few in number and consist of measurements of overall behavior with little information on the localized effects which occur in a section.

Two experiments performed as part of a recent test program are then described. Again, these give excellent confirmation of the overall validity of existing theories. However, an examination of internal strain distributions discloses a less impressive agreement between test and theory, particularly when the section is only partially yielded. In both the elastic and fully yielded regimes the test-versus-theory agreement is excellent, both overall and on a localized basis. As the overall agreement remains excellent in the partially yielded range it is concluded that the existing theories represent a good average in this case.

An examination of internal stress distributions shows that these are in agreement with the externally observed effects (such as yield penetration).

The strains at local buckling indicate that the present local buckling theory correctly predicted that the two sections tested (ASTM A441,) 14WF36 and 8WF31) would buckle locally before becoming com-

pletely strain hardened. However, it did not predict that the post-buckling strength of the sections would allow strains approaching strain-hardening to be reached before the local buckle was sufficiently severe to cause unloading.

An examination of the axial deformation showed that this effect is also subjected to the random effects of partial yielding. It also indicated that axial deformations in a section under moment and axial force can be appreciable.

The ultimate load conditions typified by the Moment M_{pc} and load P_{yc} were discussed and equations were given for their calculation in cases where the flange and web have different yield stresses and where P_{yc} and M_{pc} are linearly related. It is seen that the occurrence of local buckling will prevent the actual attainment of M_{pc} in any real section by a few percent. Experimentally both tests approached M_{pc} and, significantly, the internal strain and stress distributions were approaching their theoretical values at ultimate load.

VIII. ACKNOWLEDGEMENTS

This study is part of a general investigation "Plastic Design in High Strength Steel" currently being carried out at Fritz Engineering Laboratory, Department of Civil Engineering. Professor W. J. Eney is Head of the Civil Engineering Department and Professor L. S. Beedle is Director of the Laboratory. The investigation is sponsored jointly by the Welding Research Council, and the Department of the Navy, with funds

furnished by the American Institute of Steel Construction, The American Iron and Steel Institute, Lehigh University Institute of Research, the Bureau of Ships and the Bureau of Yards and Docks. The Column Research Council acts in an advisory capacity.

The work in this report was performed while one of the authors (Niels Gimsing) was a visiting research worker at Fritz Laboratory, and acknowledgement is made to the authorities at the Danish Institute of Technology and Lehigh University who made his stay here possible. The tests were performed by the other author with the enthusiastic assistance of Mr. R. Aglietti, to whom many thanks are due. The tests will be more generally reported in a forthcoming report of Project 297, "Plastic Design in High Strength Steel".

Both authors wish to express their appreciation of the encouragement, assistance and advice which they received from Professor Theodore V. Galambos, who is Director of Project 297, and who influenced and guided this work to its present fruition.

Miss Valerie Austin typed this report and Mr. R. Sopko did the drawings.

IX. NOMENCLATURE

A	area of cross-section
A_s	sub-area
B	section constant, equation 19
E	Young's modulus
I	moment of inertia
L	length
M	moment
M_i	internal moment
M_{pc}	ultimate value of M under thrust
P	thrust
P_i	internal thrust
P_y	$A\bar{\sigma}_y$
P_{yc}	ultimate value of P under moment
b	breadth of section
d	depth of section
e	M/P (eccentricity of load)
t	flange thickness
w	web thickness
x_s	distance of sub-area from YY axis of section
y	distance from XX axis of section
y_s	distance of sub-area from XX axis of section
z	parameter
α	ratio of tensile to compressive residual strains

β	neutral axis parameter
ϵ	strain
ϵ_o	centerline strain
ϵ_r	residual strain
ϵ_{rs}	sub-area residual strain
ϵ_{ry}	sub-area yield strain
ϵ_{rf}	flange residual strain
ϵ_y	yield strain (σ_y/E)
ϵ_c	$\sigma_{c/E}$
ϵ_w	$\sigma_{w/E}$
ϵ_t	$\sigma_{t/E}$
η	parameter
θ	rotation
σ	stress
σ_y	yield stress
σ_{yf}	flange yield stress
σ_{yw}	web yield stress
σ_c	effective yield stress of flange in compression
σ_w	effective yield stress of web in compression
σ_t	effective yield stress of flange in tension
ψ	curvature
ψ_y	yield curvature, equation 17
ψ_{av}	average curvature

TABLE 1

ECCENTRIC STUB COLUMNS TEST VARIABLES

Test No.	HT-18	HT-2	T-7	T-8
Source	Proj. 297	Proj. 297	Ref. 7	Ref. 7
Section	14WF78 (column)	8WF31 (column)	12WF36 (beam)	12WF36 (beam)
b (in.)	11.875	8.031	6.625	6.625
t (in.)	0.716	0.410	0.514	0.514
d (in.)	14.175	8.125	12.30	12.30
w (in.)	0.445	0.347	0.337	0.337
A ($in.^2$)	22.53	9.09	10.78	10.78
b/t	16.6	19.6	12.9	12.9
d/w	31.8	23.4	36.5	36.5
material	ASTM A441	ASTM A441	ASTM A7	ASTM A7
σ_{yf} (ksi)	54.2	53.4	33.9	33.9
σ_{yw} (ksi)	54.6	52.0	37.9	37.9
$bt/w(d-2t)$	1.50	1.295	0.895	0.895
σ_{rf} (ksi)	2.0	2.2	2.6	2.6
σ_{rw} (ksi)	6.0	5.7	4.7	4.7
σ_c (ksi)	52.2	51.2	31.3	31.3
σ_w (ksi)	60.6	59.7	40.5	40.5
σ_t (ksi)	56.2	55.6	36.5	36.5
L/r_x	7.9	9.5	7.0	7.0
P_y (kip) (stub column)	1198 (HT-20)	497 (HT-8)	367 (T-1)	367 (T-1)
P_y (kip)(calc)	1225	486	380	380
Transition P/P_y (eq. 18)	0.29	0.31	0.42	0.42
Load Eccentricity e/d	0.218	0.500	0.142	0.415

TABLE 2

ECCENTRIC STUB COLUMNS TEST RESULTS

	Test Number	
	HT-18	HT-2
P_{yc} (kip) Calculated	855	243
P_{yc} (kip) Test	830	234
Error	-2.9%	-3.7%
M_{pc} (kip-in) Calculated (e. P_{yc})	2640	985
M_{pc} (kip-in) Test	2585	976

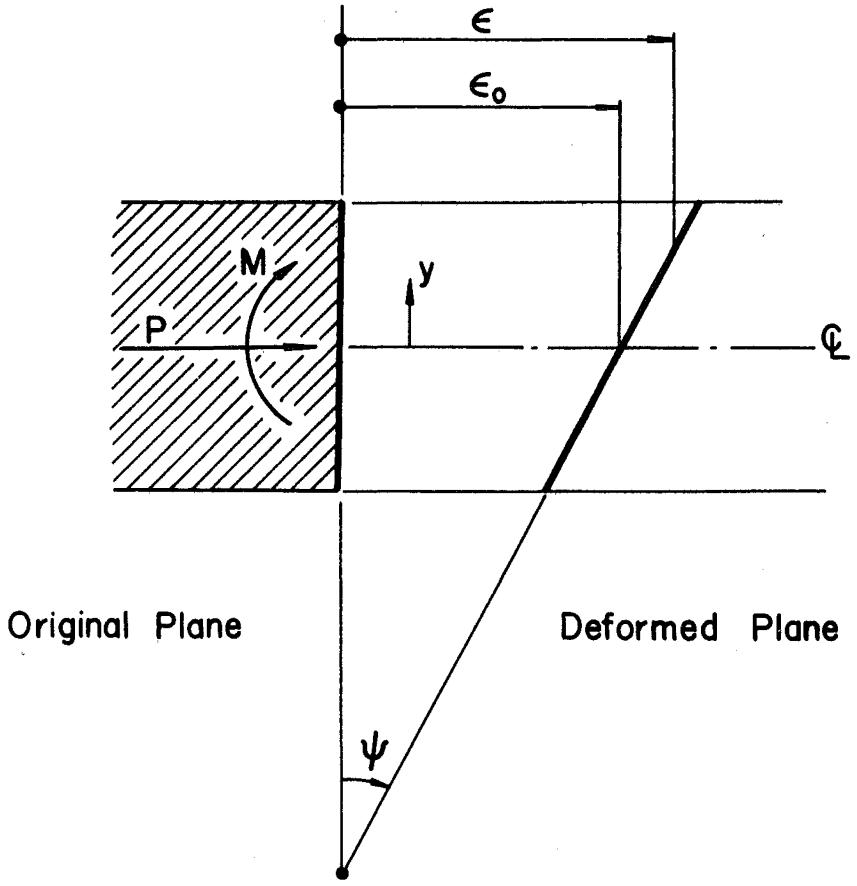

FIG. 1

DEFINITION OF SYMBOLS

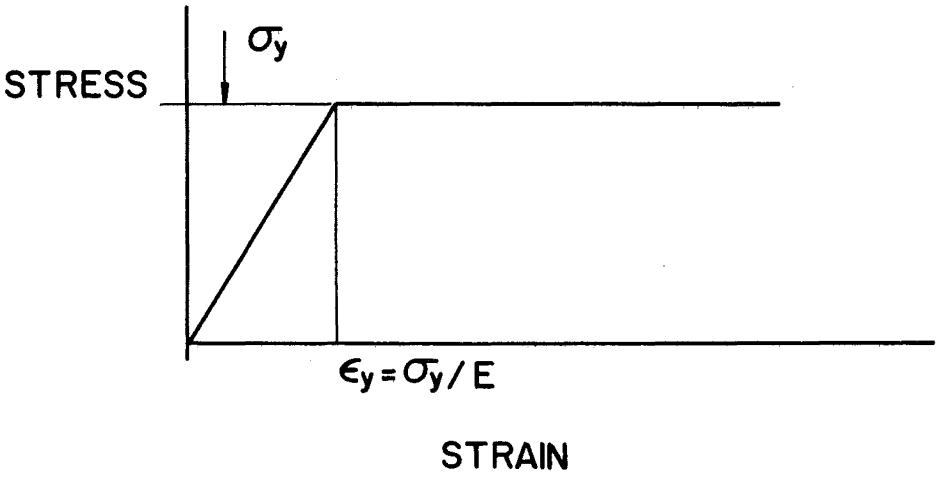

FIG. 2

STRESS STRAIN CURVE

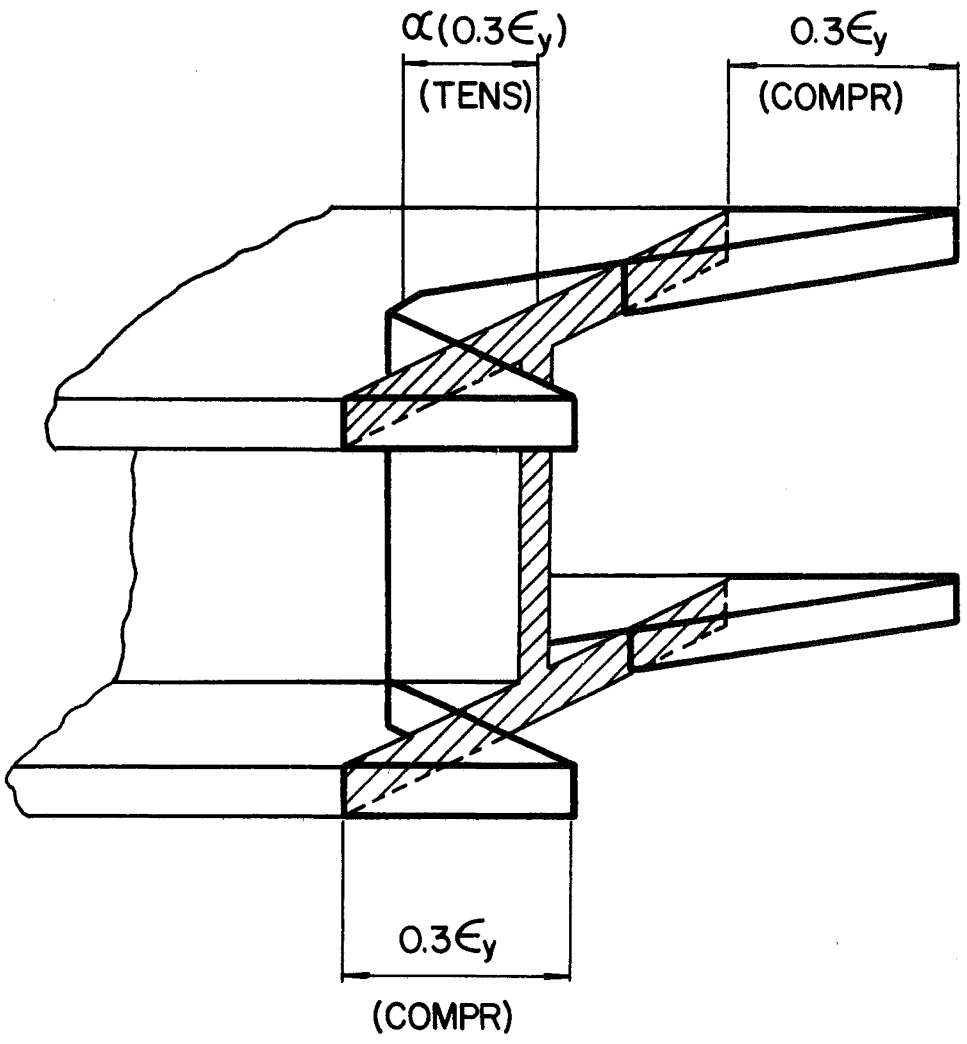

FIG. 3

RESIDUAL STRAINS

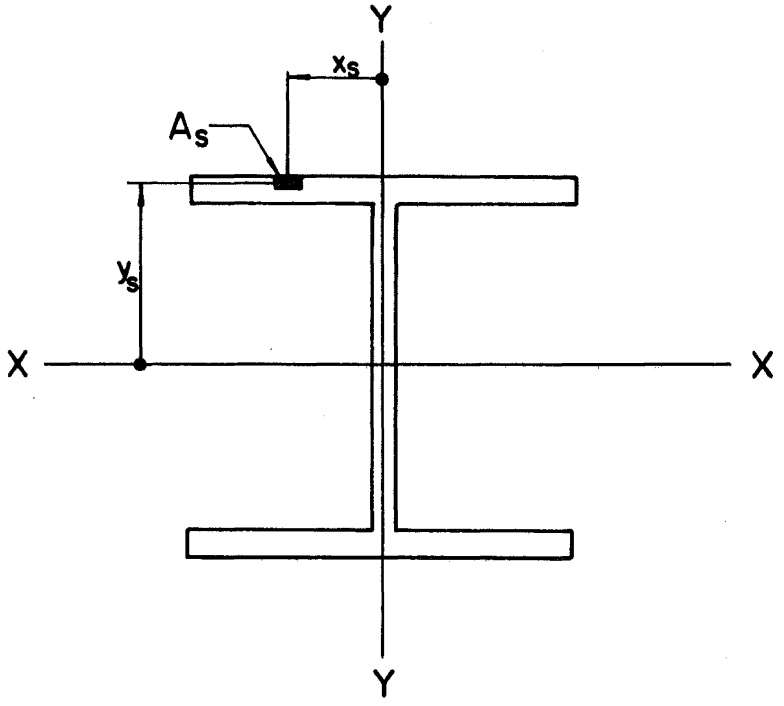

FIG. 4

SUB-AREA METHOD

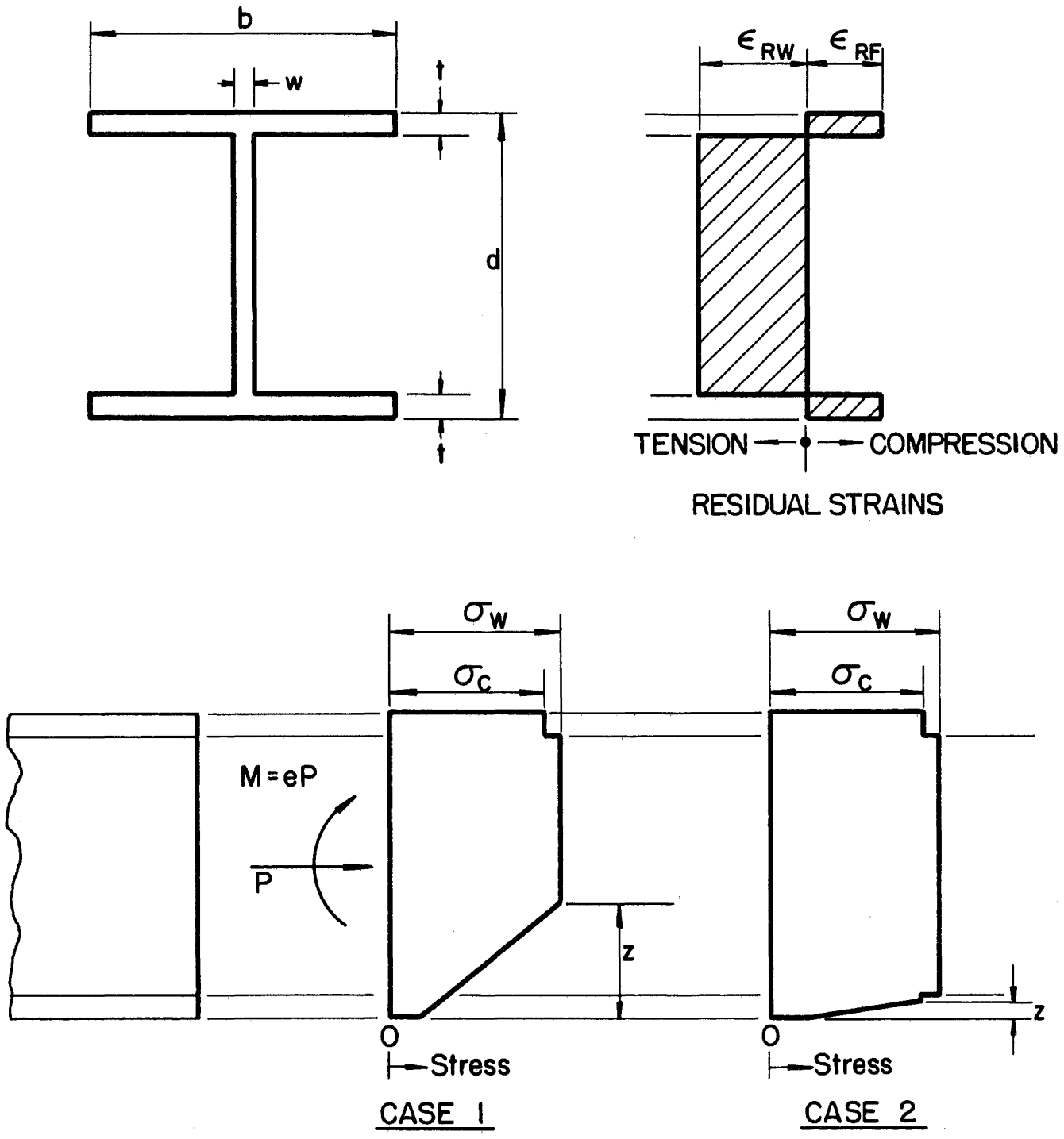

FIG. 5

STRESS-DISTRIBUTIONS

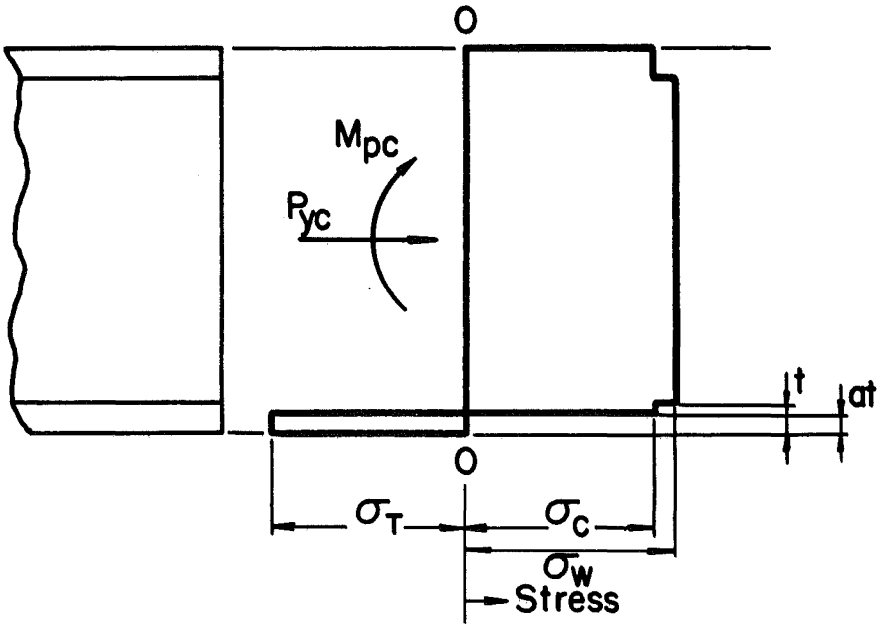

FIG. 6

ULTIMATE MOMENT STRESSES

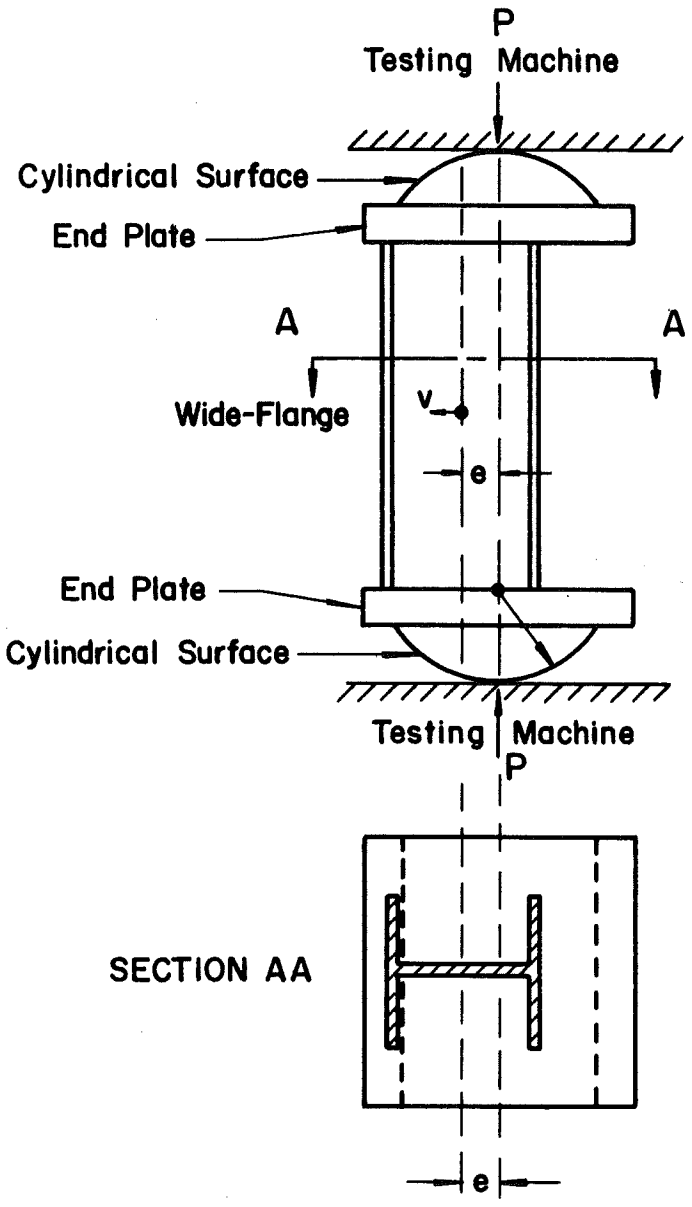

FIG. 7

TESTING ARRANGEMENT

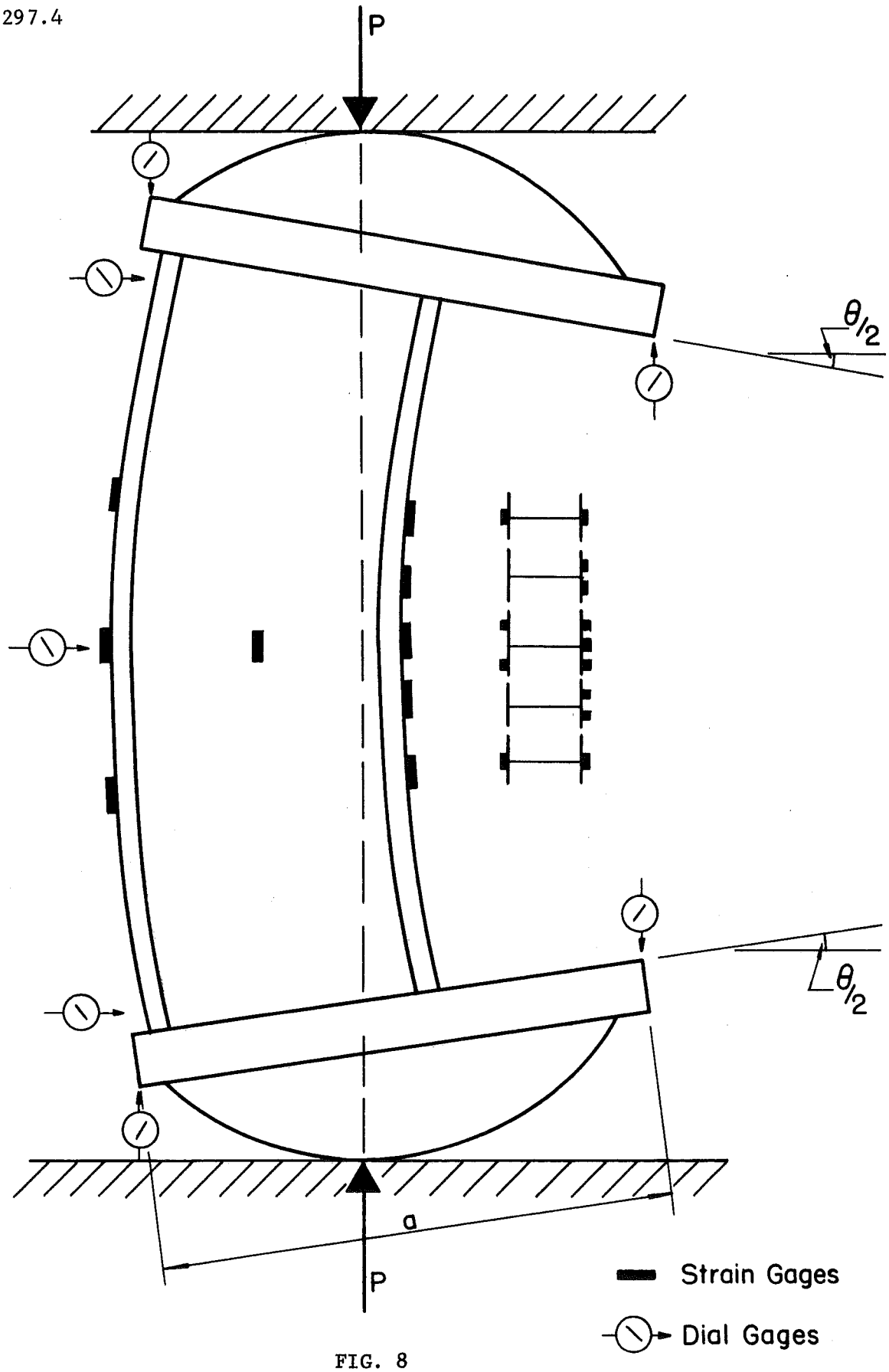

FIG. 8

INSTRUMENTATION

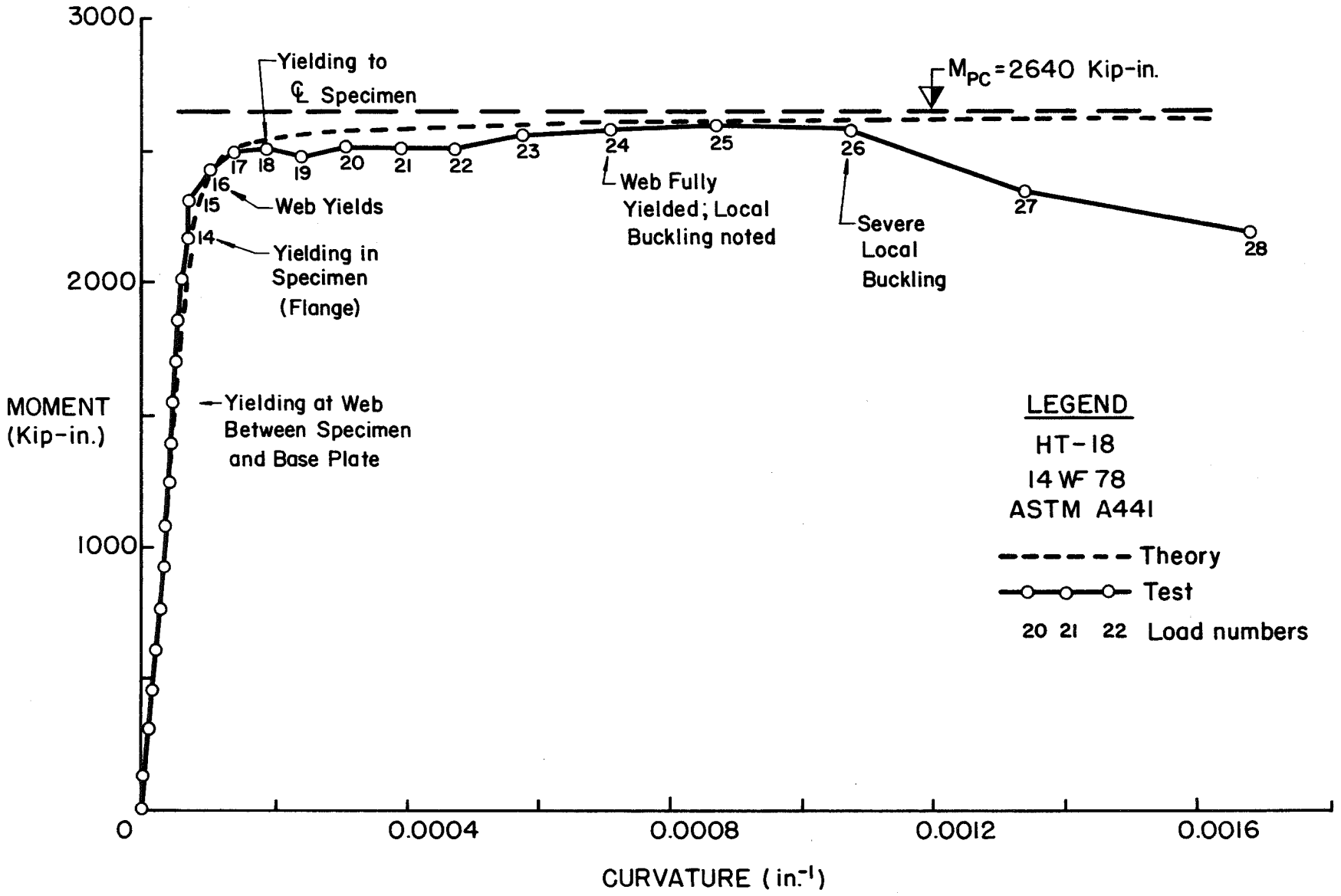

FIG. 9a

MOMENT-CURVATURE RELATION FOR TEST HT-18

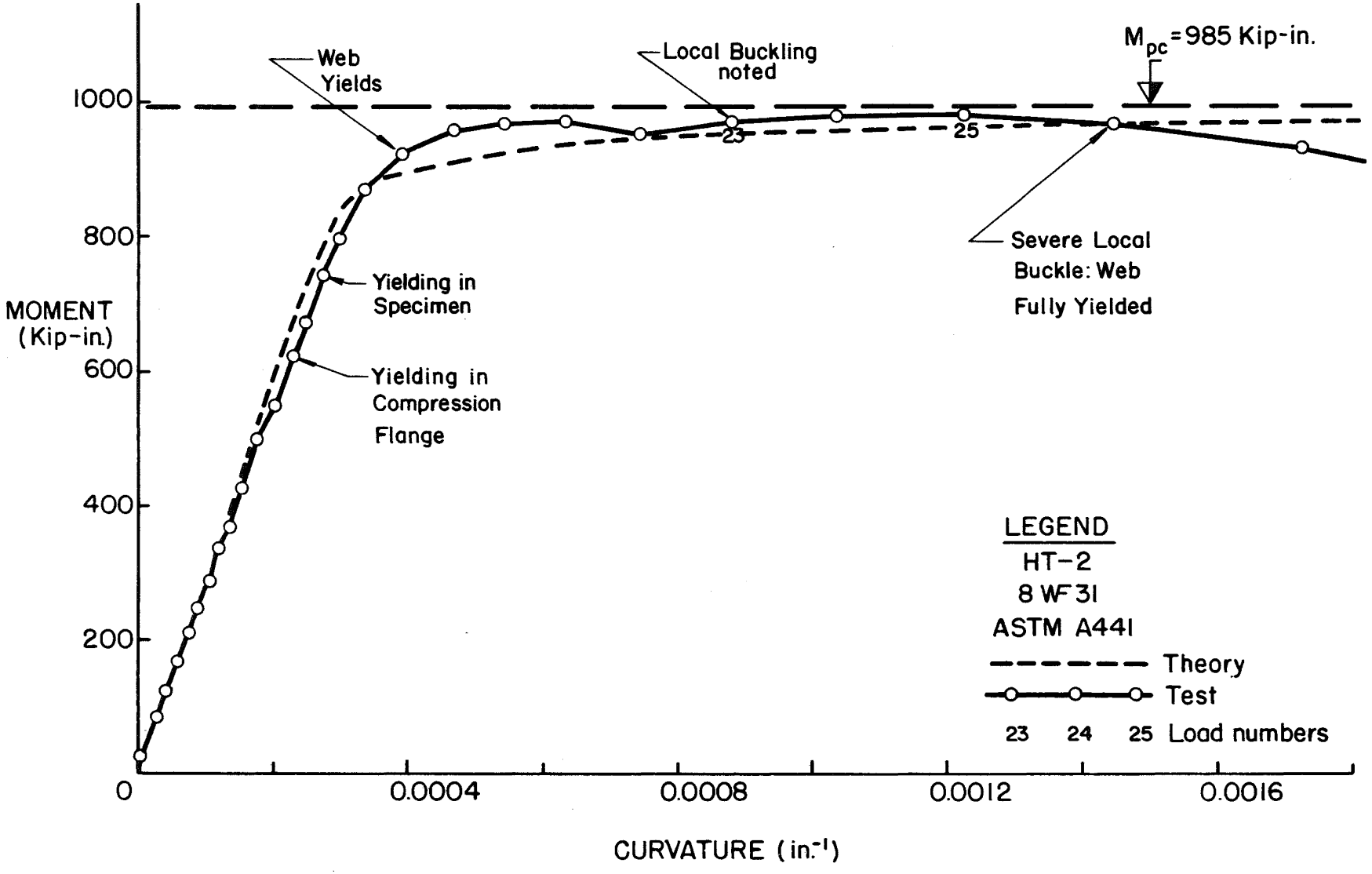

FIG. 9b

MOMENT CURVATURE RELATION FOR TEST HT-2

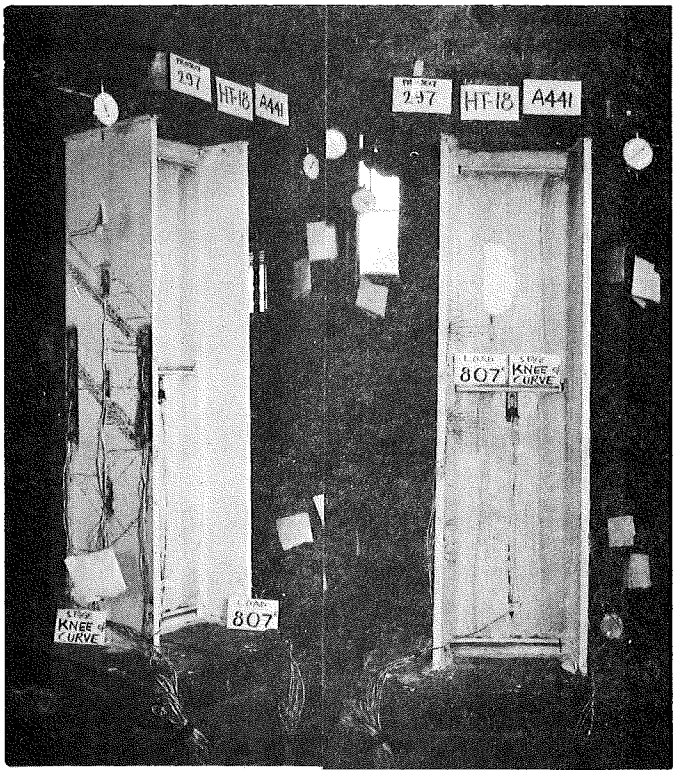

FIG. 10a
LOAD #17

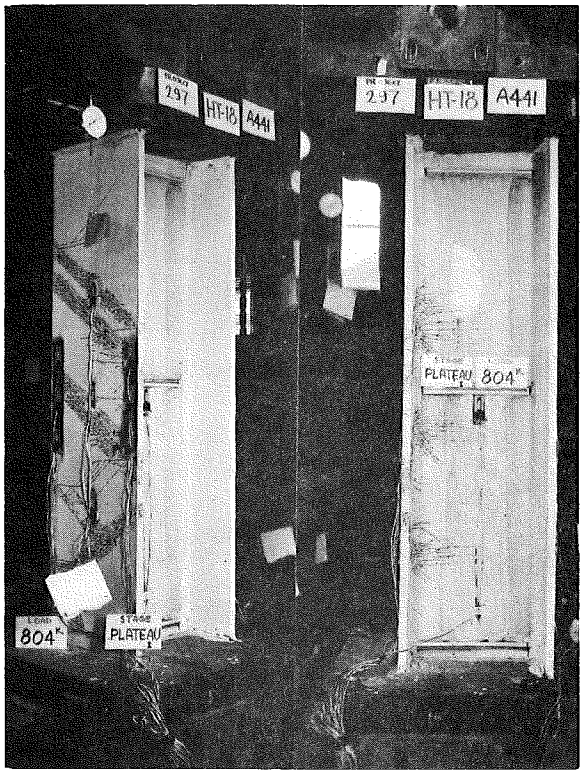

FIG. 10b
LOAD #19

FIG. 10

PHOTOGRAPH OF TEST HT-18

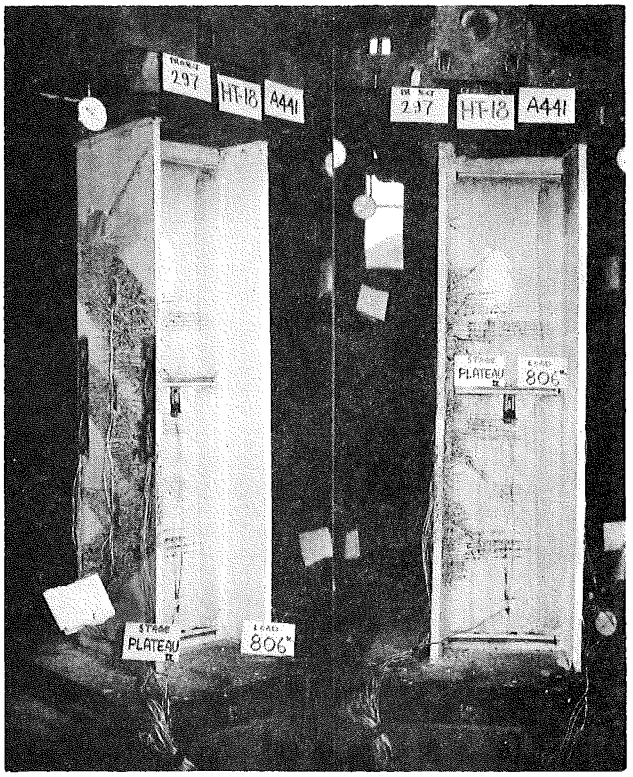

FIG. 10c
LOAD #21

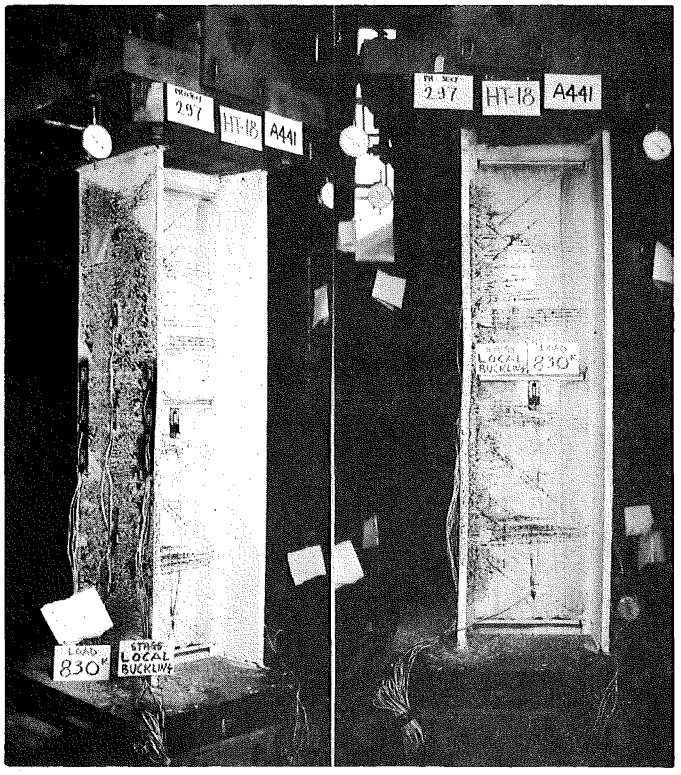

FIG. 10d
LOAD #25

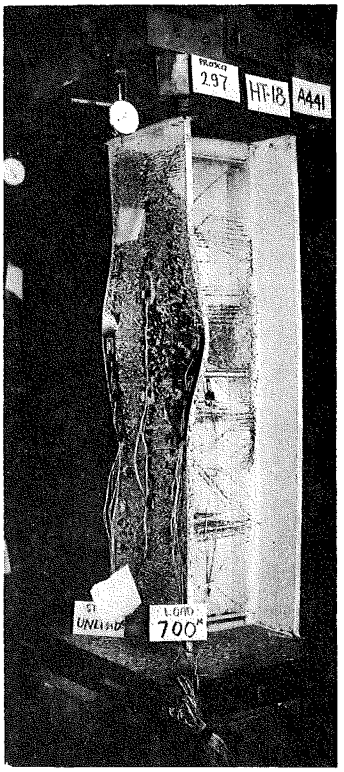

FIG. 10e
LOAD #28

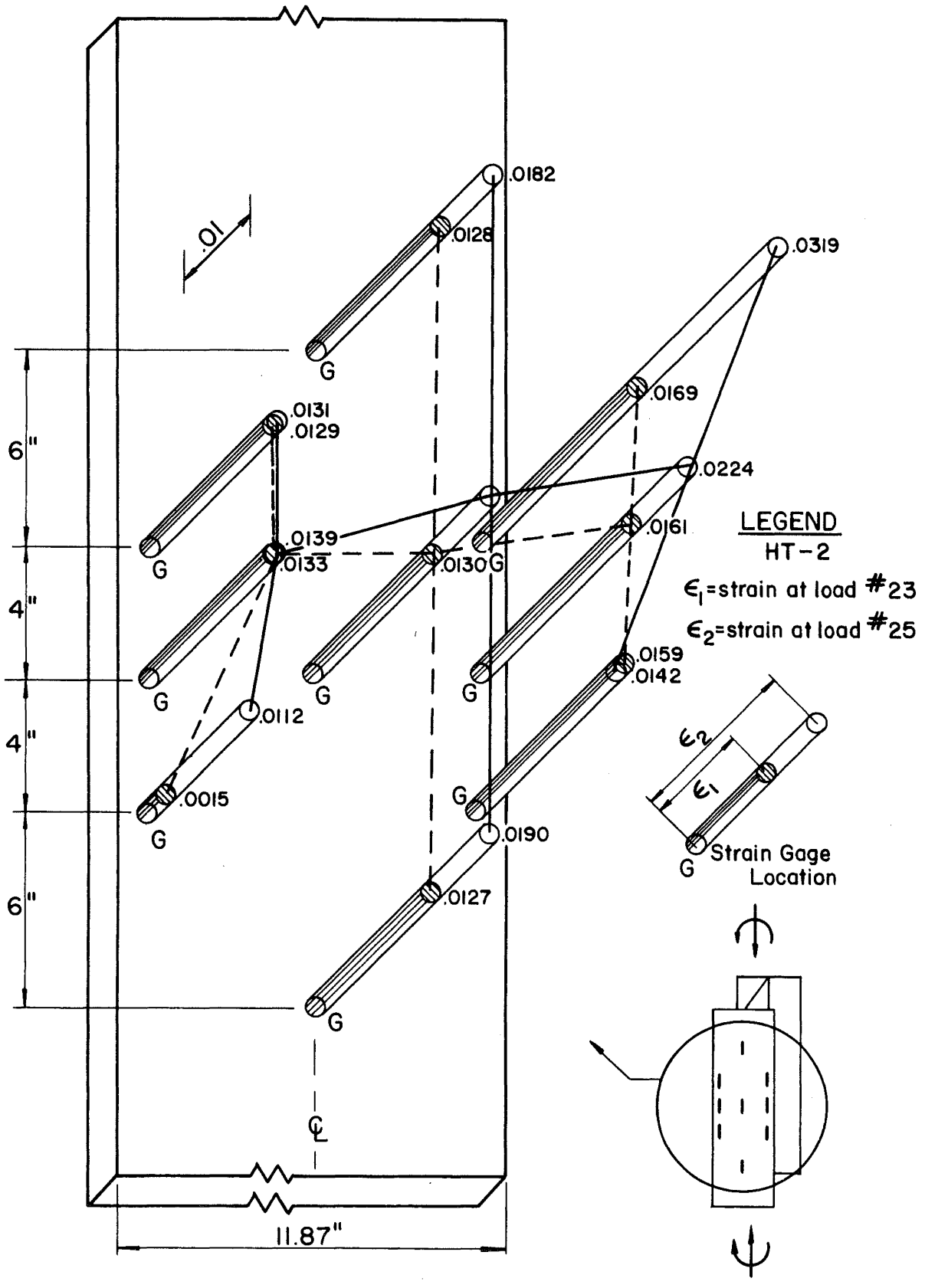

FIG. 11a

STRAINS AT LOCAL BUCKLING (TEST HT-18)

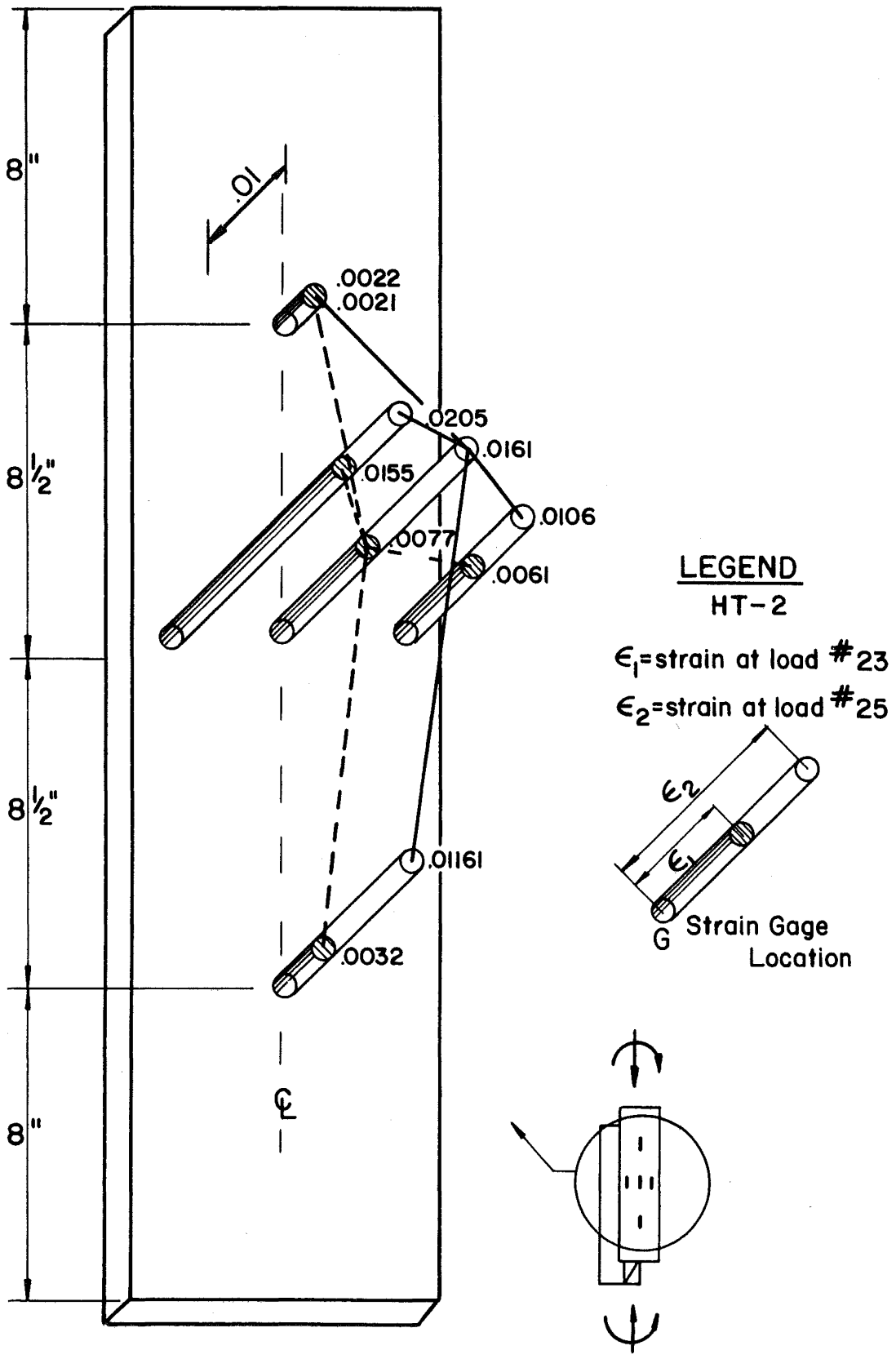

FIG. 11b

STRAINS AT LOCAL BUCKLING (TEST HT-2)

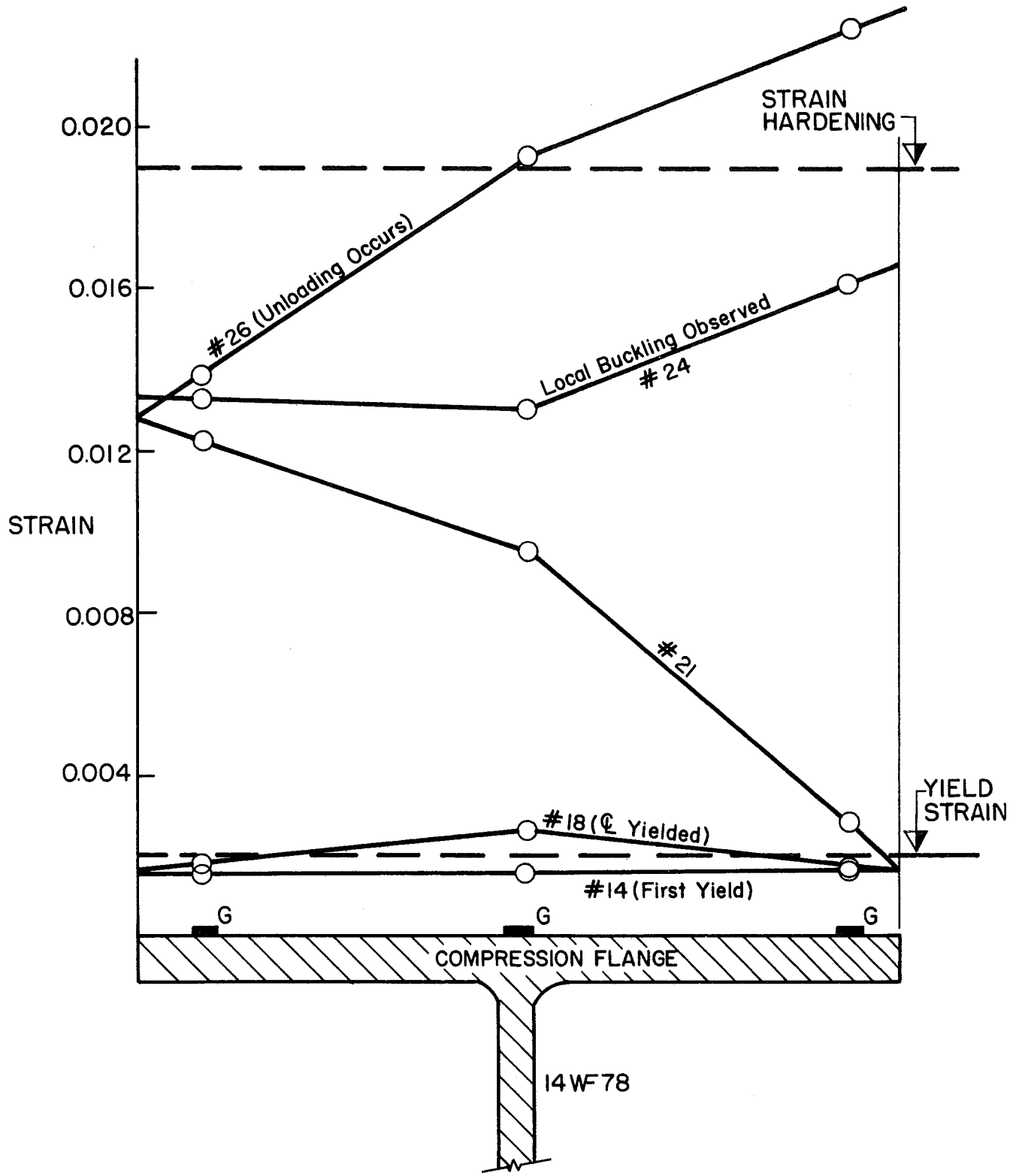

FIG. 12

STRAIN DISTRIBUTION ACROSS COMPRESSION FLANGE
AT MIDHEIGHT (HT-18)

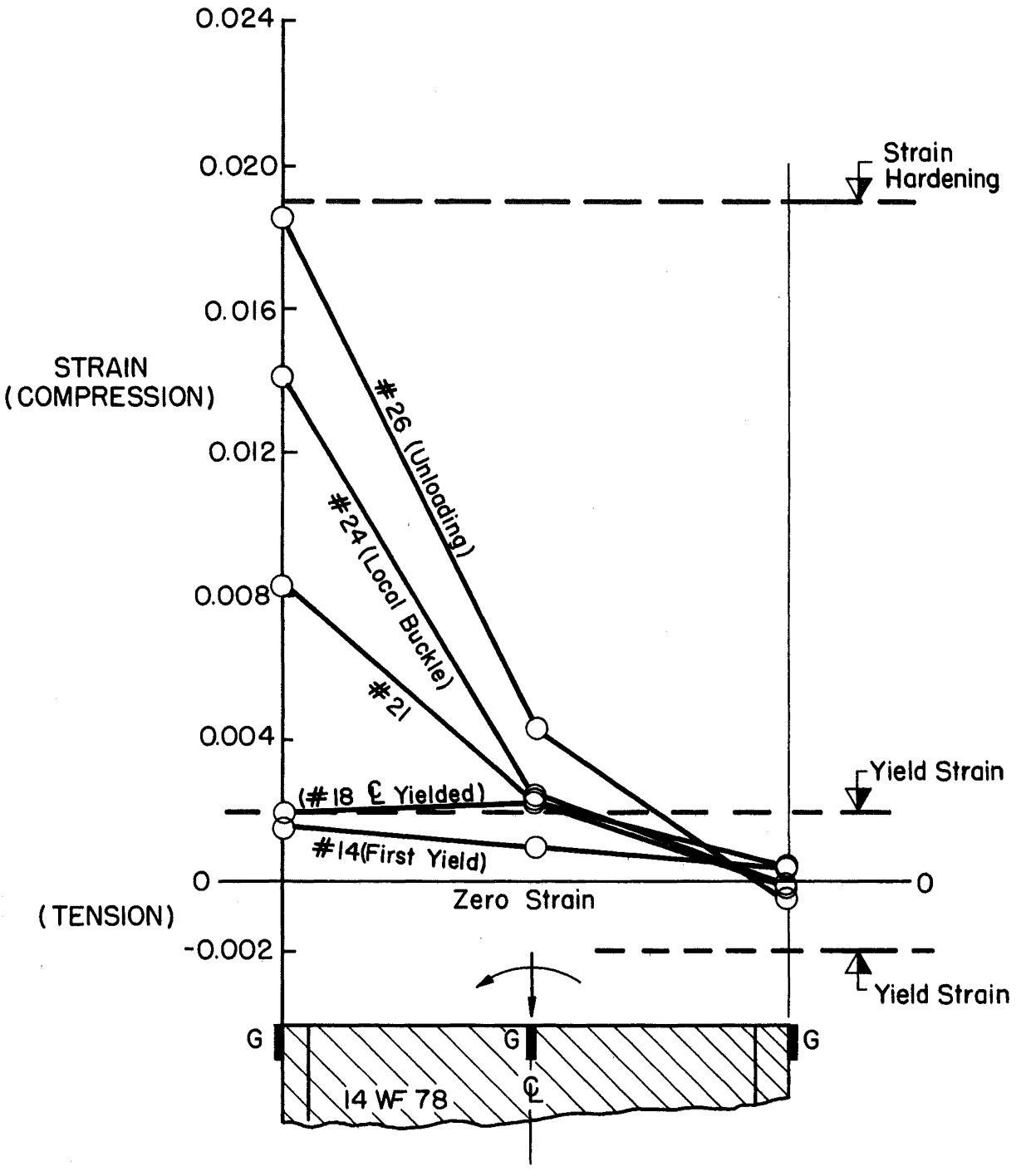

FIG. 13

STRAIN DISTRIBUTION ACROSS WEB AT MIDHEIGHT
(HT-18)

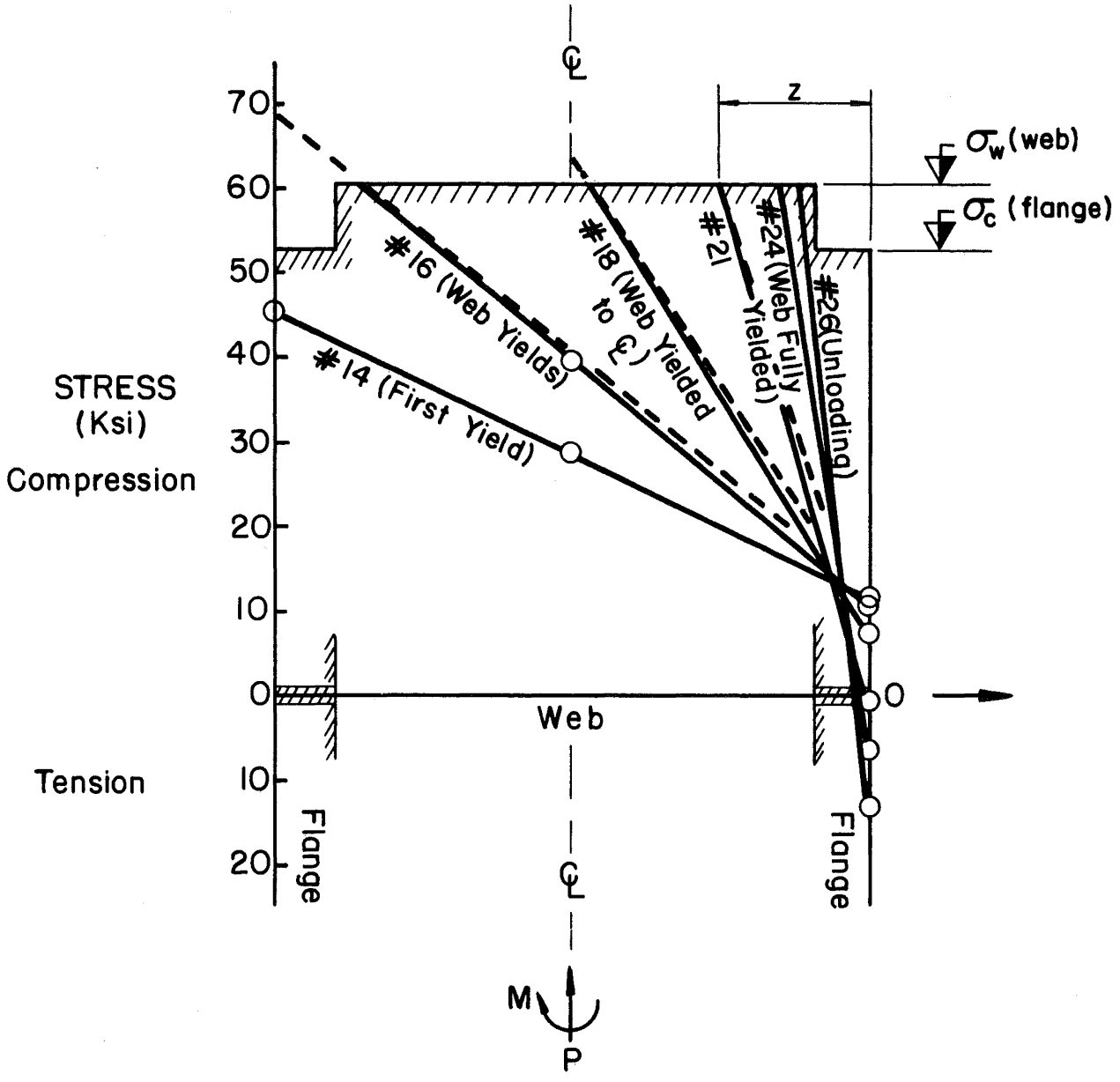

FIG. 14

STRESS DISTRIBUTION ACROSS SECTION AT MIDHEIGHT
(HT-18)

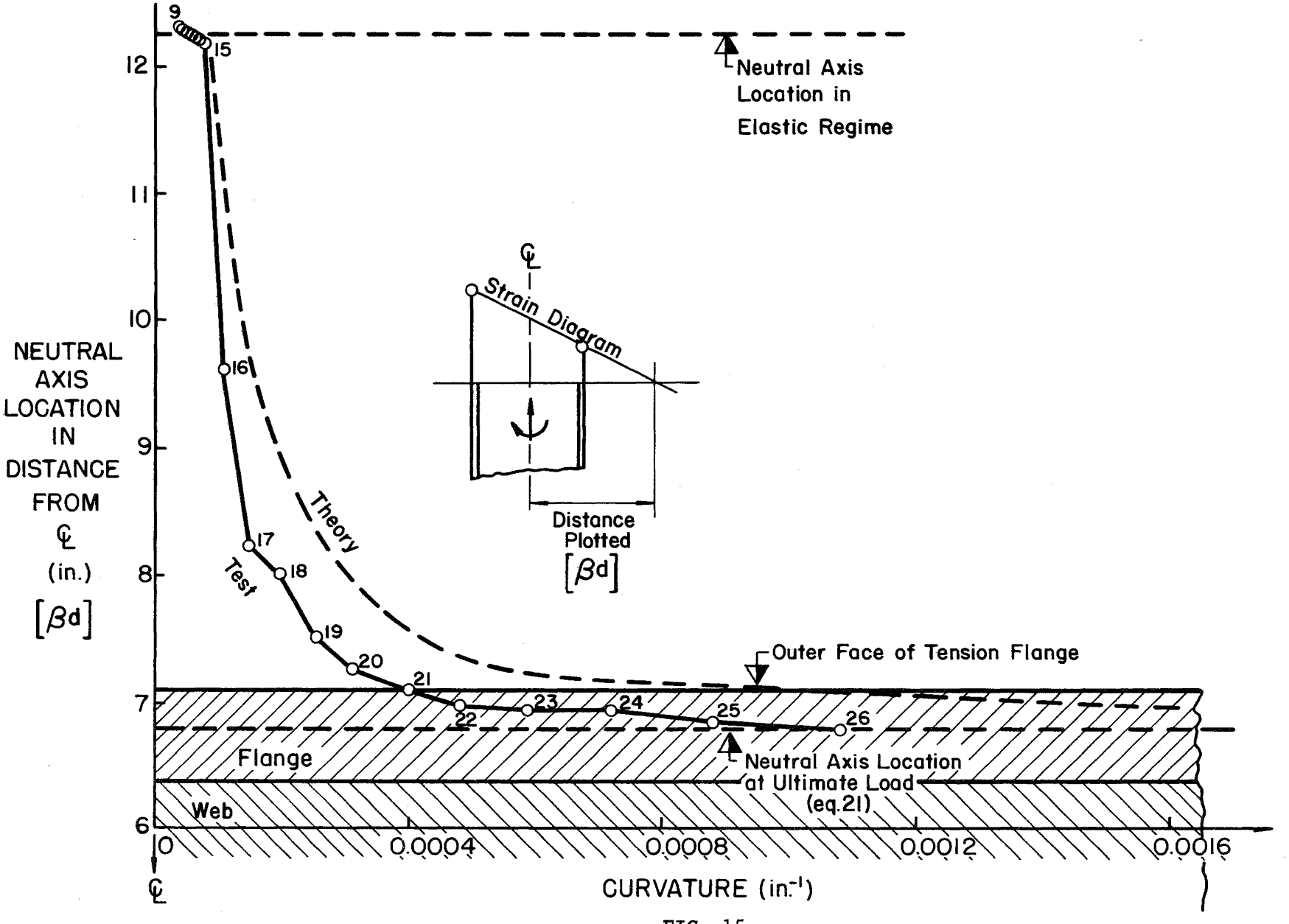

FIG. 15

VARIATION OF NEUTRAL AXIS LOCATION
(HT-18)

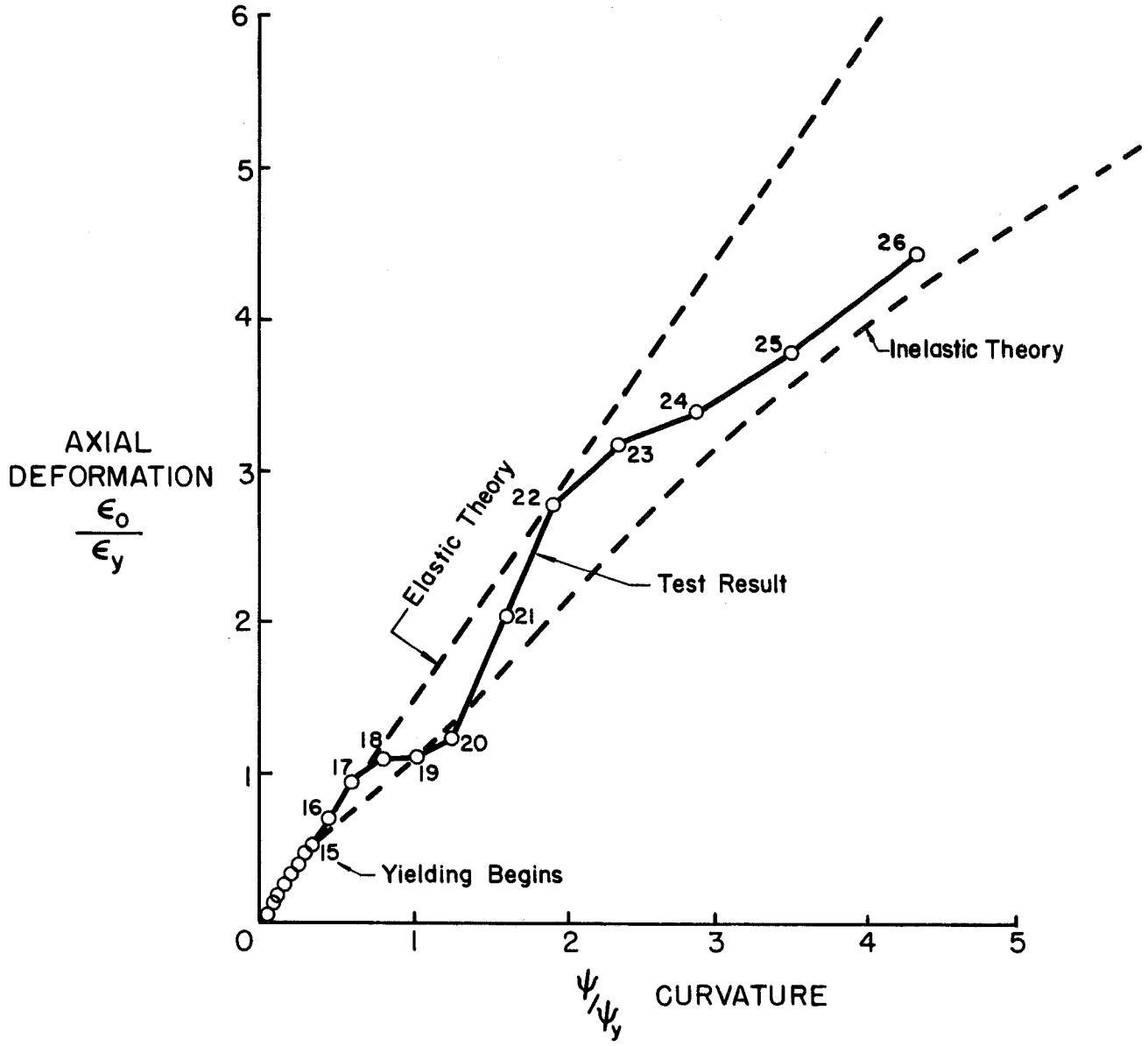

FIG. 16

RELATION BETWEEN CURVATURE AND AXIAL DEFORMATION (MIDHEIGHT, HT-18)

XI. REFERENCES

1. Sokolinkoff, J. S.
MATHEMATICAL THEORY OF ELASTICITY, McGraw-Hill, New York, (1956)

2. Roderick, J. and Phillips, I.
CARRYING CAPACITY OF SIMPLY SUPPORTED STEEL BEAMS, Res. (Engineering Structures Supplement), Colston Papers, 2(9), (1949)

3. Ketter, R. L., Kaminsky, E. and Beedle, L. S.
PLASTIC DEFORMATIONS OF WIDE FLANGE BEAM-COLUMNS, Trans. ASCE, 120, p. 1028 (1955)

4. Fukumoto, Y. F.
MOMENT-CURVATURE-THRUST PROGRAM FOR WIDE-FLANGE SHAPES, Fritz Laboratory Report 205A.37, Lehigh University (August 1963)

5. Birnsteil, C. and Michalos, J.
ULTIMATE LOAD OF H COLUMNS UNDER BIAXIAL BENDING, Proc. ASCE, 89(ST2), (April 1963)

6. BEEDLE, L. S.
PLASTIC DESIGN OF STEEL FRAMES, John Wiley & Sons, New York, (1958)

7. Driscoll, G. C. and Beedle, L. S.
THE PLASTIC BEHAVIOR OF STRUCTURAL MEMBERS AND FRAMES, Welding Journal, 36(6), p. 275s, (June 1957)

8. Hendry, A. W.
AN INVESTIGATION OF THE STRENGTH OF CERTAIN WELDED PORTAL FRAMES IN RELATION TO THE PLASTIC METHOD OF DESIGN, Struct. Engr., 28(12), (December 1950)

9. Huber,A.
FIXTURES FOR TESTING PIN-ENDED COLUMNS, ASTM Bulletin 234, p. 41, (December 1958)

10. ASCE-WRC
COMMENTARY ON PLASTIC DESIGN, ASCE Manual No. 41, Chapter 6, (1961)

11. Haaijer, G.
PLATE BUCKLING IN THE STRAIN-HARDENING RANGE, Proc. ASCE, 83 (EM2), (April 1957